Tuning Optimization of Ring Resonator Delays for Integrated Optical Beam Forming Networks

Yuan Liu, Adam Wichman, *Member, IEEE*, Brandon Isaac, Jean Kalkavage, *Member, IEEE*, Eric J. Adles, *Senior Member, IEEE*, Thomas R. Clark, *Senior Member, IEEE, Member, OSA*, and Jonathan Klamkin, *Senior Member, IEEE, Senior Member, OSA*

***Abstract*—Comprehensive tuning optimization of an integrated optical ring resonator (ORR) based 1 × 4 optical beam forming network (OBFN) for W-band millimeter wave (mmW) phased arrays is reported. The OBFN chip is implemented using a ultralow loss silicon nitride technology and a two stage binary tree topology. The delay responses of a single- and multiORR delay line were carefully measured, and the results agree well with a lossless theoretical model. Tuning of an ORR was calibrated and verification experiments were performed to verify the tuning accuracy. A flattened delay response for a 3-ORR delay line was achieved, demonstrating a bandwidth of 6 GHz and dynamic tuning range of 209 ps, which corresponds to a phase shift of 33.4π for an 80-GHz signal. A larger bandwidth can be achieved by reducing the dynamic tuning range. The result is promising for high data rate mmW communications with beamforming.**

***Index Terms*—Microwave photonics, millimeter wave communication, optical ring resonators, phased arrays, photonic integrated circuits, true time delays.**

I. Introduction

MILLIMETER wave (mmW) frequencies are attractive for broadband point-to-point wireless communications due to the large available bandwidth, compact antenna size, and potential use in commercial 5G applications [1]. The W band, ranging from 75 GHz to 110 GHz, is particularly suitable for long-haul communications due to the relatively low atmospheric attenuation of less than 1 dB/km in clear weather and 2 dB/km in light rain. For comparison, a loss of greater than 20 dB/km is observed for frequencies near 60 GHz [2]. Microwave Photonics (MWP) is a frequency agile technology for microwave signal generations over all RF bands. Particularly, in W band, MWP is more promising for mmW generation at such high frequency than traditional RF circuits due to the low loss of optical fiber and the immunity to electromagnetic interference [1], [3]. In combination with true time delays (TTDs), which mitigate the beam squint issue incurred by using phase shifters [4], MWP is particularly suitable for beam forming for mmW phased array antennas (PAA) with high bit rate communication. An 88 GHz photonic based mmW beamsteering PAA was implemented using discrete TTD elements, and a data rate of 10 Gb/s with $\pm 35^\circ$ beamsteering angle was demonstrated [5]. Due to the short wavelength nature of mmWs and the small size PAA, the delay should be precisely controlled to obtain good beam quality, therefore high-performance TTD technologies are required.

The development of integrated photonics technology in the last decade makes integrated MWP for optical beam forming networks (OBFNs) more cost efficient, compact, and light weight. Furthermore, it enables integration of optical signal processing circuits [6]. Integrated optical delay lines are the key elements for OBFNs, and thus far, two methods have been implemented. The first is realized by switching between delay lines with various lengths [7]. This method requires relatively simple controls, but it only supports discrete delays and the delay resolution is limited by the shortest delay line. The second method uses all pass filters such as optical ring resonators (ORRs), and is more powerful due to the small chip footprint and the ability to continuously tune the delay. Recently, researchers have successfully demonstrated ORR-based OBFNs with different platforms [8]–[12], and a delay of 0.63 ns with a bandwidth of 2 GHz targeting Ku-band PAA was reported [13], [14]. ORRs could also be combined with switchable delay lines to achieve high delays while maintaining the continuously tuning ability [15]. For ORR-based OBFNs, in order to achieve wide bandwidth TTDs and mitigate fabrication variations, precise calibrations and tuning should be applied to all the rings in the network. However, to our best knowledge, no such work has been reported.

In this paper, we present a comprehensive tuning optimization of an integrated ORR-based 1×4 OBFN for W-band mmW generation and beamsteering targeting the up-conversion approach described in [5], [16]. The OBFN was realized with a two-stage binary-tree topology utilizing a low-loss silicon nitride waveguide technology [17]. The group delay response of ORR-based delay lines was carefully calibrated and optimized using the theoretical model. An improved measurement setup is also discussed to monitor the delay spectrum in real time for tuning multiple ORR delay lines. For the remainder of the paper, the operating principle and the chip design are described in

Manuscript received April 26, 2017; revised August 4, 2017; accepted September 29, 2017. Date of publication October 12, 2017; date of current version November 16, 2017. *(Corresponding author: Yuan Liu.)*

Y. Liu and J. Klamkin are with the Electrical and Computer Engineering Department, University of California, Santa Barbara, CA 93106 USA (e-mail: yuanliu@umail.ucsb.edu; klamkin@ece.ucsb.edu).

A. Wichman is with the School of Engineering, Brown University, Providence, RI 02912 USA (e-mail: adam_wichman@brown.edu).

B. Isaac is with the Materials Department, University of California, Santa Barbara, CA 93106 USA (e-mail: brandonjisaac@gmail.com).

J. Kalkavage, E. Adles, and T. Clark are with the Johns Hopkins University Applied Physics Laboratory, Laurel, MD 20723 USA (e-mail: jean.kalkavage@jhuapl.edu; eric.adles@jhuapl.edu; Thomas.Clark@jhuapl.edu).

Color versions of one or more of the figures in this paper are available online at http://ieeexplore.ieee.org.

Digital Object Identifier 10.1109/JLT.2017.2762641

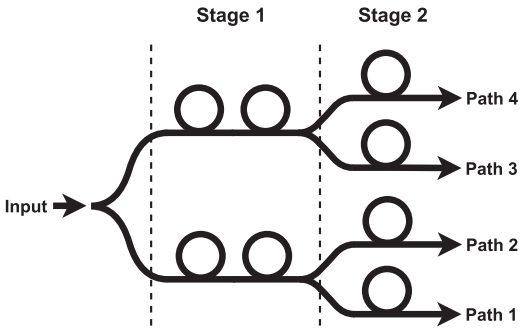

Fig. 1. Schematic of an 1 × 4 ORR-based two-stage binary tree OBFN.

Section II. Section IV shows the experimental setup for the group delay characterization and Section V provides and discusses the experimental results. Conclusions are made in Section VI.

II. Operating Principle

Fig. 1 shows a schematic of the 1 × 4 two-stage binary tree OBFN used in this work. The OBFN employs ORRs as the basic delay elements in each of the paths. A single ORR exhibits a bell-shaped group delay spectrum, with the peak centered at the resonance frequency (f_r) and minima at the anti-resonant frequencies (f_{ar}), as depicted in Fig. 2(a). Given that ultra-low loss waveguides have been developed in the past years [18], we may express the delay spectrum of a single ORR analytically with a lossless ring waveguide assumption as [19]

$$\tau_g(\lambda) = \frac{\kappa \cdot \tau_r}{2 - \kappa - 2\sqrt{1-\kappa} \cdot \cos\left(2\pi\tau_r \cdot \frac{c}{\lambda} + \phi\right)} \tag{1}$$

where κ is the power coupling coefficient, ϕ is the phase offset from the ring resonance, and τ_r is the round-trip propagation delay, which is equal to the reciprocal of the free spectral range (f_{FSR}). Given a specific dimension of an ORR, κ determines the shape of the curve, i.e., the bandwidth and the maximum and minimum delays, whereas the phase shift, ϕ, determines the resonance frequency of the ORR. With increasing κ, as shown in Fig. 2(a), the maximum group delay at f_r decreases rapidly whereas the minimum group delay at f_{ar} increases gradually. The group delay spectrum therefore flattens with increasing κ and the bandwidth increases. When κ becomes equal to 1, the bandwidth becomes infinity, the delay response becomes a flat line and is equal to the round trip delay of the ring. An inherent trade-off exists between the delay bandwidth and peak delay value.

The group delay and TTD bandwidth of a single ORR may be limited. However, cascading multiple ORRs can provide wider bandwidth and large group delay tuning if the coupling coefficient and phase shifter of each ORR are properly tuned, as illustrated in Fig. 2. The group delay of three cascaded rings is equal to the sum of the individual ones. These attributes are desirable for high-frequency wide-bandwidth communications. However, based on our previous work[20], the flattened group delay response exhibits delay ripple, or deviation from the desired delay across frequency, which may distort the output microwave signal

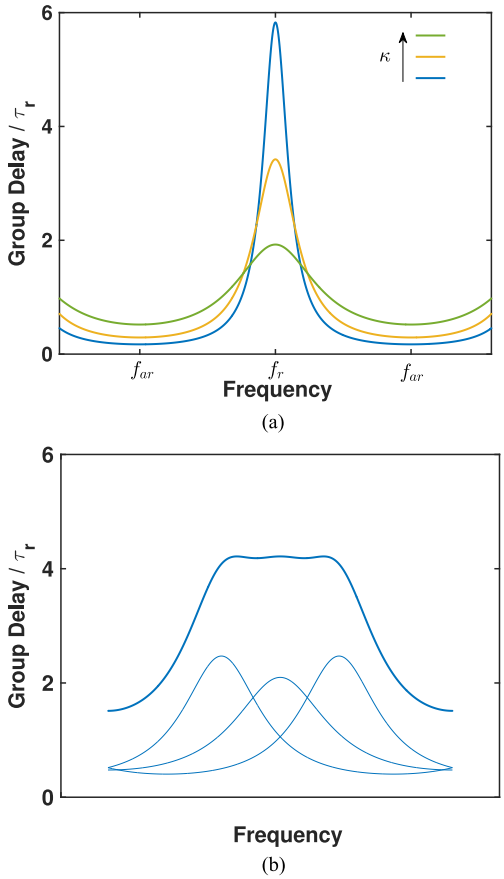

Fig. 2. (a) Single ORR bell-shaped group delay spectra for different values of κ. (b) Three cascaded ORR flattened delay response. f_r and f_{ar} refer to resonance frequency and anti-resonance frequency; τ_r refers to the round-trip propagation delay of the ring.

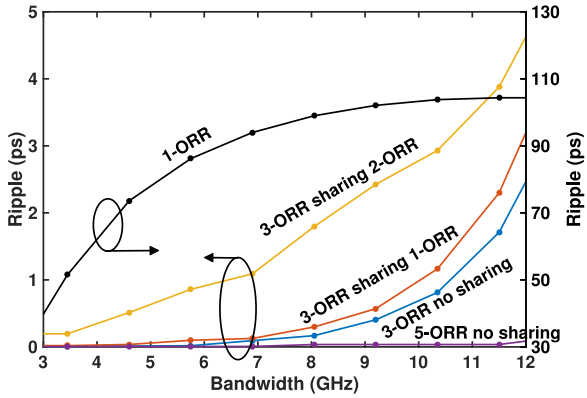

Fig. 3. Simulation demonstrating trade-offs between ripple, bandwidth, and number of cascaded rings for delay line with 1-ORR, 3-ORR, 5-ORR, 3-ORR sharing 1-ORR, and 3-ORR sharing 2-ORR. The FSR is 23 GHz and target delay is 147.8 ps. The ripple is characterized as the maximum delay deviation from the target delay over a given bandwidth.

and possibly lead to system operation failure. Inherent trade-offs exist between bandwidth, ripple, delay, and number of cascaded rings. The trades-offs for an ORR with $FSR = 23$ GHz and target delay of 147.8 ps for 1-, 3- and 5-ORR delay lines are shown in Fig. 3 where the ripple is defined as the maximum delay deviation from the target delay over a given bandwidth.

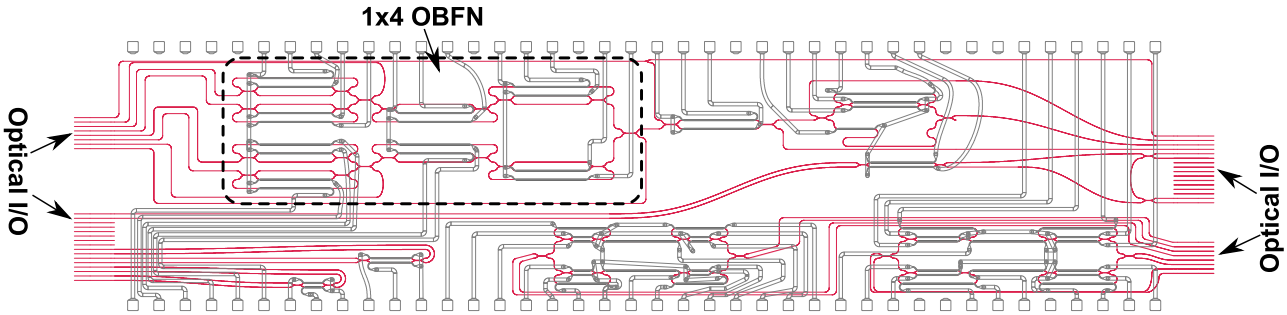

Fig. 4. Layout of the OBFN chip with footprint of 8×32 mm^2 comprising a 1×4 OBFN, fiber array compatible edge couplers, and other test structures.

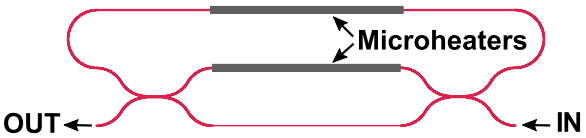

Fig. 5. Close-up of layout of an ORR.

As shown, cascading more rings could improve the ripple and bandwidth considerably. Moreover, the OBFN employs a two-stage binary tree topology in which two adjacent delay paths share delay elements within the first stage. This topology could reduce the number of ORRs to be controlled at the cost of deteriorating the flatness of the group delay response. Fig. 3 shows the ripple bandwidth trade-off of a two-stage binary tree topology with 3-ORR delay line as well as a comparison to that of a one-stage binary tree topology. As observed, having more rings shared within a stage reduces the system complexity but at the expense of larger ripple. For prototyping purposes, we chose a 3-ORR delay line two-stage binary tree topology with 2-ORR sharing in the first stage. As will be shown, this minimizes system complexity while maintaining acceptable ripple.

III. Device Design

The OBFN chip was realized for C-band operation and fabricated with an ultra low-loss silicon nitride technology [17] demonstrating low optical loss and an potential to handle high optical power up to 120 mW without severe non-linear effect occurs [21], which is ideal for high-power millimeter waves emittion with a large signal-to-noise ratio. Fig. 4 shows the layout of the chip that has an overall footprint of 8×32 mm^2. The chip has an ORR based two-stage binary tree 1×4 OBFN as discussed earlier. The ORRs are designed to have a FSR of 22 GHz. They are connected to waveguides through a symmetric Mach-Zehnder interferometer (MZI) based tunable coupler, as illustrated in Fig. 5. A 2-mm long chromium heater is placed on one arm of the MZI for tuning the coupling of light to the ORR so that $0 \sim 1$ of coupling coefficient can be achieved. A 2-mm heater is also placed on the race track of each ORR as a phase shifter to tune the resonance frequency.

At both edges of the chip, two waveguide arrays are included with a pitch of 127 μm so that the chip can be pigtailed to a standard commercial fiber array for optical input and output. These waveguides are also tapered to match the mode size of the fiber array in order to improve the coupling efficiency. In addition, some MZI and high order optical sideband filters test structures are included on the chip. All of the heater leads are routed to metal pads at the edges of the chip so that a 40-pin probe can be used to connect current sources to the heaters.

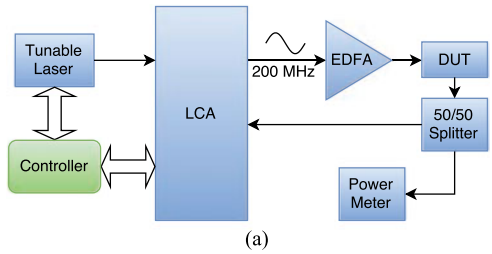

(a)

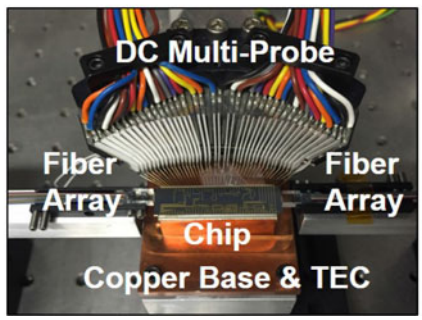

(b)

Fig. 6. (a) Group delay measurement setup. (LCA: lightwave component analyzer; DUT: device under test; EDFA: erbium-doped fiber amplifier), (b) Testbed for the OBFN chip with fiber-array I/O and a customized 40-pin probe.

IV. Experimental Setup

The test setup for the OBFN chip characterization is shown in Fig. 6. The chip was mounted on a copper stage with thermal conductive compound and the temperature is stabilized by a thermoelectric cooler. Light is coupled to and from the chip with two standard commercial fiber arrays as shown in Fig. 6(b). A 40-pin probe was used to contact the pads at the edge of the chip. A custom breakout box was utilized so that source meters could tune heaters using standard connectors.

A modulation phase shift method was used to measure the group delay response as shown in Fig. 6(a). A tunable laser (Yenista, TUNICS T100S-HP) emitting in the C-band was coupled to a Lightwave Component Analyzer (LCA)

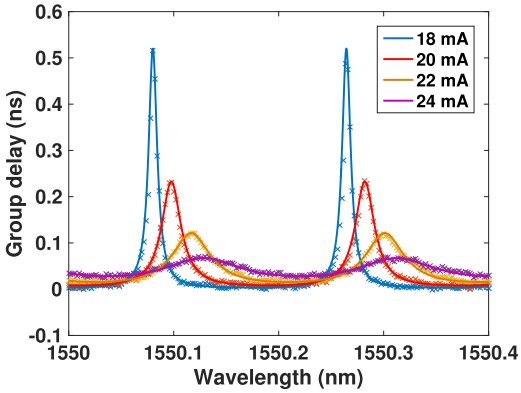

Fig. 7. Measured delay spectra and the corresponding fits for single ORR at various current levels. The crosses denote the measured delays, whereas the solid curves denote the fits that use the model in (1).

(Hewlett-Packard, HP8703A). The LCA modulates the intensity with a constant 200 MHz sinusoidal signal. The light was then amplified by an erbium-doped fiber amplifier (EDFA) (IPG Photonics, EAR-2K-C) and coupled to the device and then split with a 50/50 fiber coupler. One output of the coupler was input to a power meter for monitoring, and the other output was coupled back to the LCA for measurement of the group delay. The EDFA was used to adjust the power level of the light input to the LCA in order to maximize the accuracy of the measurement. The LCA measures the phase shift of the modulated signal due to the delay in the external optical path. The group delay in terms of the phase shift can be expressed as follows:

$$\tau_g(\lambda) = \frac{\Delta\phi(\lambda)}{2\pi f_0} \tag{2}$$

where λ is the wavelength, $\Delta\phi$ is the measured phase shift and f_0 is the modulation frequency. Moreover, tuning ORRs requires a fast measurement of the group delay spectrum. This is achieved by synchronizing the light source and LCA with a controller. Consequently, a speed of 1.6 s per sweep over 0.5 nm is achieved, enabling real-time tuning of ORRs. Absolute measurement of the ORR group delay is not possible using this method due to the additional delay from external fibers and waveguides on the chip. However, these extra delays can be accounted for by fitting the measured delay spectrum using the model provided by (1) plus a constant delay term, which represents the additional delays.

V. Results and Discussion

The coupling coefficient of each ORR can be varied from 0 to 1 by tuning the current of the corresponding MZI coupler. The delay response of a delay line can be measured by sweeping the laser wavelength. Fig. 7 shows the group delay response of a single ORR for different current levels over two FSRs. The measured data is fit using the model in (1) to extract the tuning parameters (κ and ϕ) and FSR, as well as to eliminate additional delays. The excellent fit indicates the accuracy of the lossless model for the ORRs. Increasing the current increases the coupling coefficient while flattening the bell-shape delay spectrum, as expected. This demonstrates the inherent trade-off between the delay bandwidth and peak delay value. The FSR of the ORR was measured to be 23.1 GHz, which is close to the designed FSR.

TABLE I
A Typical Look-Up Table for a 23 GHz FSR 3-ORR Delay Line

Delay (ps)	Ripple (ps)	κ_1	κ_2 and κ_3	ϕ_2 or $-\phi_3$ (rad)
208.7	1.30	0.8154	0.7539	0.9249
182.6	0.48	0.8803	0.8261	1.0618
165.2	0.15	0.9269	0.8821	1.1806
147.8	0.05	0.9642	0.9359	1.3808
139.1	0.01	0.9792	0.9624	1.5590
113.0	0.25	0.9815	0.9490	2.8025
95.7	0.33	0.9752	0.8001	2.5066
78.3	0.19	0.9867	0.6588	2.7576
69.6	0.20	0.9891	0.4912	2.5032
26.1	2.32	0	0.6705	2.9489
8.7	0.82	0	0.3035	3.0273

κ_x and ϕ_x refer to the coupling coefficient and phase offset from the resonance of ring$_x$, as described in (1); ϕ_1 is set to zero in the simulation. Ripple defines as the maximum deviation from the desired delay across the bandwidth.

A notable shift of delay spectrum is observed while tuning the coupler. This shift originates from the phase shift of light through the MZI coupler. The transmission of the MZI coupler was studied utilizing transfer matrix techniques given by

$$T = \begin{bmatrix} T_{11} & T_{12} \\ T_{21} & T_{22} \end{bmatrix} \tag{3}$$

$$T_{11} = (1-\kappa)e^{-j\Delta\psi} - \kappa \tag{4}$$

$$T_{12} = T_{21} = 2\sqrt{\kappa(1-\kappa)}\cos\frac{\Delta\psi}{2}e^{-j(\frac{\Delta\psi}{2}+\frac{\pi}{2})} \tag{5}$$

$$T_{22} = (1-\kappa) - \kappa e^{-j\Delta\psi} \tag{6}$$

where κ is the coupling coefficient of directional coupler in the MZI, and $\Delta\psi$ is the phase difference between two MZI arms, which is proportional to the square of heater current. (3)–(6) indicate that tuning the MZI will not only change the coupling coefficient of the ORR, but also induce a phase shift as a function of tuning current, which can be interpreted as a shift in the delay spectrum.

The group delay response formed by cascading multiple ORRs should be optimized as flat as possible to overcome beam squint, which is an important issue for wideband communications. To be specific, an 1 ps delay ripple could induce a 30° phase deviation in the wavefront of an 80 GHz signal. In our previous work, we studied the inherent trade-offs between bandwidth, ripple, and delay for ORR-based time delays using a standard genetic algorithm. The genetic algorithm is a global optimization algorithm for nonlinear problems. Meanwhile, we built a look-up table of coupling coefficient and phase offset to minimize the ripple as well [20]. A typical look-up table for a 23 GHz FSR 3-ORR delay line is shown in Table I. Careful calibration of a single ORR was performed in order to precisely control the rings using the look-up table. Fig. 8 shows the measured group delay spectra for a single ORR under

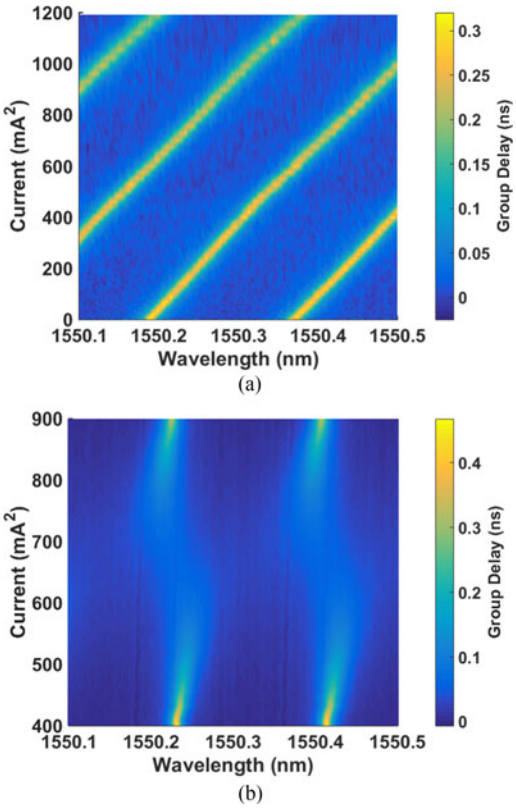

Fig. 8. Measured delay spectra of a single ORR for various tuning currents for (a) phase shifter and (b) MZI coupler.

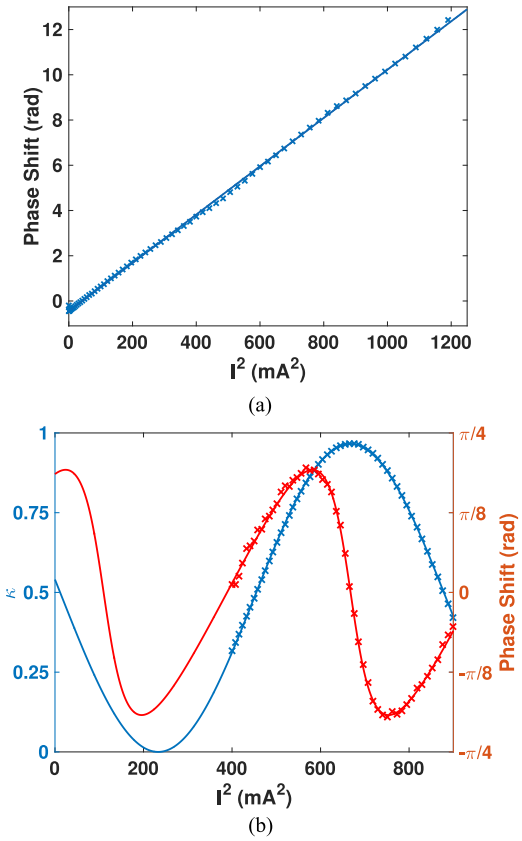

Fig. 9. Parameters (crosses) extracted from measured delay spectra, and their corresponding curve fits (solid lines) as a function of current squared. (a) Phase shift of the ORR phase shifter. (b) Coupling coefficient (blue) and phase shift (red) of the ORR MZI coupler.

different phase tuning currents and coupling tuning currents. The parameters (κ and ϕ) are extracted by fitting the data utilizing the model in (1) and plotted in Fig. 9. Since the change of refractive index is proportional to the power dissipated in the heaters, the phase shift induced by the ORR phase shifter should be proportional to the square of the current. Fig. 9(a) shows the measured response of the ORR phase shifter. The extracted tuning efficiency is of 5.3π rad/W. Ideally, the ring coupling coefficient is determined by the cross transmission (T_{12}) of the MZI coupler and has a cosinusoidal squared relation with respect to the square of current, and the MZI induced phase shift given by the argument of T_{11} should have a linear relation. However, as indicated in Fig. 9(b), the coupling coefficient does not reach 1 and the phase shift is not perfectly linear with the current squared, which can attribute to the imperfections of the 50/50 couplers of the MZI. Taking the coupling coefficient of couplers into account, the model was able to fit the data well as shown and the coupling coefficient κ was extracted as 0.6. A look-up table was then built for tuning the ORR after the calibrations.

Verification was performed to test the accuracy of the ORR tuning look-up table. The group delay spectra for various coupling coefficients with a given resonant frequency were measured, as shown in Fig. 10(a). The measurement indicates that the phase shift induced by the MZI coupler is fully compensated and the resonant frequencies of all the delay spectra are aligned. Fig. 10(b) compares the target coupling coefficient with the measured coupling coefficient extracted utilizing the same fitting method. In spite of a small offset, this figure shows a strong consistency between the measured and expected coupling coefficient. The verification demonstrates an accurate calibration and controllability for tuning the group delay of the ORR.

Due to the fabrication variation, the initial statuses of the rings on the chip are not exactly the same. Fig. 11 shows the initial group delay response of multi-ORR delay line with three identical rings, which exhibits the delay spectrum of each ring with various phase-shifts and coupling-coefficients. After applying the calibration method to every ORR in the OBFN, the resonance frequency and coupling coefficient of each ORR could be individually and precisely tuned. However, the OBFN exhibited a thermal crosstalk that reduces the tuning accuracy when attempting to simultaneously tune all the ORRs in a delay path. Therefore, in addition to using the simulation data set from Table I to directly set the ORR state for flattened delay responses, we used the simulated delay response as a reference and manually precisely tuned the ORRs to compensate the offset induced by the thermal cross talk. Fig. 12(a) shows the simulated delay responses (solid curves) and measured delay responses (points) for a 3-ORR delay line. Comparing with Fig. 11, we show that we are able to precisely control the delay spectra and that measured results agree well with simulation results. A flattened group delay response of a 3-ORR delay line with a bandwidth of >6 GHz and a dynamic tuning range of 209 ps was achieved with the delay response ripple less than 1.3 ps, which corre-

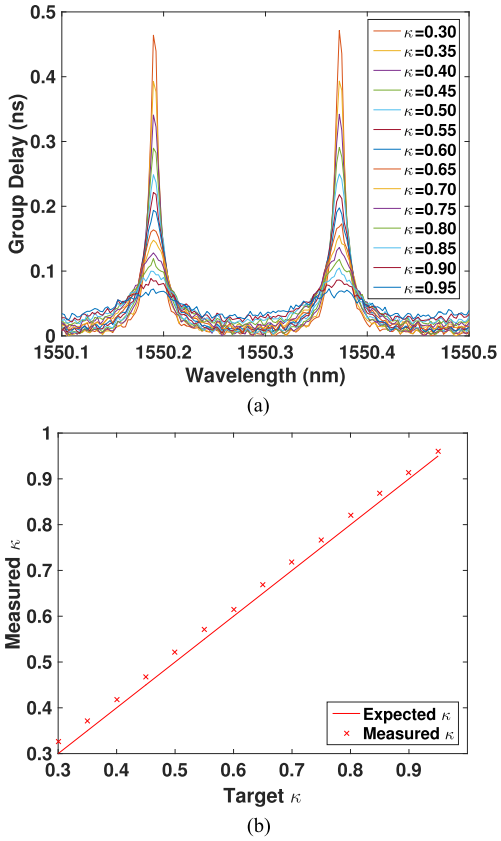

Fig. 10. Verification of calibration. (a) Measured delay spectra for a given central wavelength and various coupling coefficients using the calibration table. (b) Comparison between expected and measured coupling coefficients.

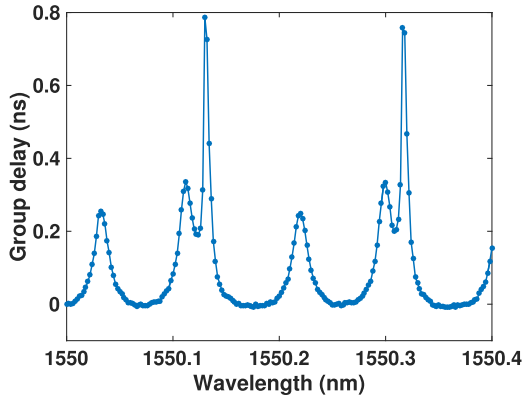

Fig. 11. The initial group delay spectrum for a 3-ORR delay line without tuning.

sponds to a phase shift of 33.4π for an 80-GHz signal. For half wavelength dipole antenna arrays at this frequency, this delay tuning range could feed a large scale PAA up to 1×33 1-D or 16×16 2-D array for a 180^{o} of beamsteering angle. A larger scale of the PAA is available if a smaller beamsteering angle is required. The normalized power transmission spectra of the 3-ORR delay line is shown in Fig. 12(b), which indicates that the delay line loss is less than 3.5 dB and the loss variation within 6.7 GHz bandwidth of each delay configuration is less than 1 dB. The total power consumption of heaters for the 3-ORR line with this tuning range varies from 1.25 W to 2.57 W. A larger bandwidth can be achieve by reducing dynamic tuning range.

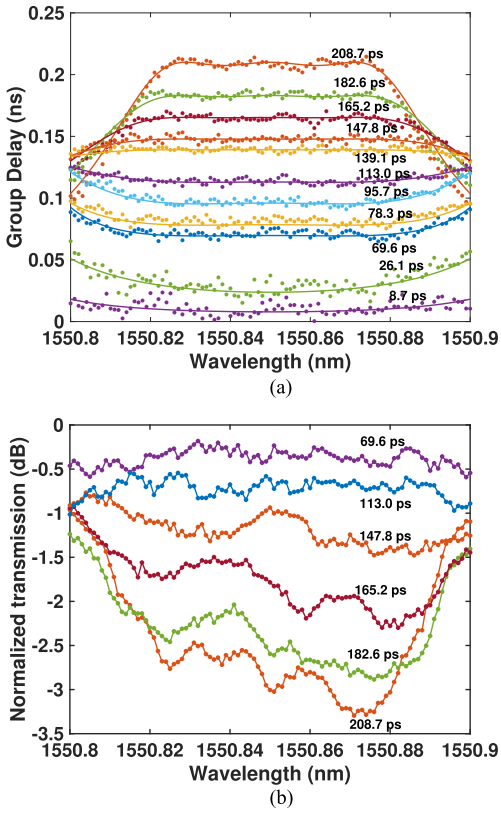

Fig. 12. (a) Measured group delay spectra (the points denote raw measured delays, whereas the solid curves denote theory) and (b) normalized power spectra for 3-ORR delay line with optimized tuning.

VI. Conclusion

In this paper, we report a comprehensive tuning optimization of an integrated 1×4 OBFN for W-band mmW generation and beam steering based on ORR delay elements. The group delays of a single- and multi-ORR delay line in the OBFN were measured. The experimental results agree with theoretical models very well and the lossless model is shown to be accurate. The tuning of single ORRs was carefully calibrated and a verification experiment was performed to verify the accuracy of the calibration. A flattened delay response of a 3-ORR delay line was achieved with a bandwidth of 6 GHz and a dynamic tuning range of 209 ps, which is promising for mmW beam forming with high data rate transmission. This delay line can be readily extended to applications in other RF frequencies. In future work, beam steering and data transmission experiments at W band will be performed to evaluate the OBFN circuit at various data rates.

References

[1] J. A. Nanzer, A. Wichman, J. Klamkin, T. P. McKenna, and T. R. Clark, "Millimeter-wave photonics for communications and phased arrays," *Fiber Integr. Opt.*, vol. 34, no. 4, pp. 159–174, 2015.

[2] J. Wells, "Faster than fiber: The future of multi-G/s wireless," *IEEE Microw. Mag.*, vol. 10, no. 3, pp. 104–112, May 2009.

[3] D. Marpaung, C. Roeloffzen, R. E. R. Heideman, A. Leinse, S. Sales, and J. J. E. Capmany, "Integrated microwave photonics," *Laser Photon. Rev.*, vol. 7, no. 4, pp. 506–538, 2013.

[4] I. Frigyes and A. J. Seeds, "Optically generated true-time delay in phased-array antennas," *IEEE Trans. Microw. Theory Techn.*, vol. 43, no. 9, pp. 2378–2386, Sep. 1995.

[5] T. P. McKenna, J. A. Nanzer, and T. R. Clark, "Photonic beamsteering of a millimeter-wave array with 10-Gb/s data transmission," *IEEE Photon. Technol. Lett.*, vol. 26, no. 14, pp. 1407–1410, Jul. 2014.
[6] S. Iezekiel, M. Burla, J. Klamkin, D. Marpaung, and J. Capmany, "RF engineering meets Optoelectronics: Progress in integrated microwave photonics," *IEEE Microw. Mag.*, vol. 16, no. 8, pp. 28–45, Sep. 2015.
[7] R. L. Moreira *et al.*, "Integrated ultra-low-loss 4-Bit tunable delay for broadband phased array antenna applications," *IEEE Photon. Technol. Lett.*, vol. 25, no. 12, pp. 1165–1168, Jun. 2013.
[8] F. Xia, L. Sekaric, and Y. Vlasov, "Ultracompact optical buffers on a silicon chip," *Nature Photon.*, vol. 1, no. 1, pp. 65–71, 2007.
[9] J. Cardenas *et al.*, "Wide-bandwidth continuously tunable optical delay line using silicon microring resonators," *Opt. Express*, vol. 18, no. 25, pp. 26525–26534, 2010.
[10] J. Xie, L. Zhou, Z. Zou, J. Wang, X. Li, and J. Chen, "Continuously tunable reflective-type optical delay lines using microring resonators," *Opt. Express*, vol. 22, no. 1, pp. 817–823, 2014.
[11] Y. Liu *et al.*, "Single ring resonator delays for integrated optical beam forming networks," in *Proc. IEEE Int. Top. Meeting Microw. Photon.*, 2016, vol. 7, pp. 321–324.
[12] N. Tessema *et al.*, "Radio beam-steering via tunable Si_3N_4 optical delays for multi-Gbps K-band satellite communication," in *Proc. Opt. Fiber Commun. Conf.* Washington, D.C.: OSA, 2016, Paper W3K.4. [Online]. Available: https://www.osapublishing.org/abstract.cfm?uri=OFC-2016-W3K.4
[13] L. Zhuang *et al.*, "Novel ring resonator-based integrated photonic beamformer for broadband phased array receive antennas–part II: Experimental prototype," *J. Lightw. Technol.*, vol. 28, no. 1, pp. 19–31, 2010.
[14] C. Roeloffzen, P. van Dijk, D. Marpaung, M. Burla, and L. Zhuang, "Development of a broadband integrated optical beamformer for Kuband phased array antennas," in *Proc. 34th ESA Antenna Workshop*, 2012, pp. 3–5.
[15] X. Wang, L. Zhou, R. Li, J. Xie, L. Lu, and J. Chen, "Nanosecond-range continuously tunable silicon optical delay line using ultra-thin silicon waveguides," in *Proc. Conf. Lasers Electro-Optics*. Washington, D.C.: OSA, 2016, Paper STu1G.5. [Online]. Available: https://www.osapublishing.org/abstract.cfm?uri=cleo_si-2016-STu1G.5
[16] T. P. McKenna, J. A. Nanzer, and T. R. Clark, "Experimental demonstration of photonic millimeter-wave system for high capacity point-to-point wireless communications," *J. Lightw. Technol.*, vol. 32, no. 20, pp. 3588–3594, 2014.
[17] R. G. Heideman, A. Leinse, M. Hoekman, F. Schreuder, and F. H. Falke, "TriPleX^{TM}: The low loss passive photonics platform: Industrial applications through Multi Project Wafer runs," in *Proc. 2014 IEEE Photonics Conf.*, 2014, pp. 224–225.
[18] J. F. Bauters *et al.*, "Ultra-low-loss high-aspect-ratio Si3N4 waveguides," *Opt. Express*, vol. 19, no. 4, pp. 3163–3174, 2011.
[19] G. Lenz, B. Eggleton, C. Madsen, and R. Slusher, "Optical delay lines based on optical filters," *IEEE J. Quantum Electron.*, vol. 37, no. 4, pp. 525–532, Apr. 2001.
[20] Y. Liu, A. Wichman, B. Isaac, J. Kalkavage, E. Adles, and J. Klamkin, "Ring resonator delay elements for integrated optical beamforming networks: Group delay ripple analysis," in *Proc. Adv. Photon. 2016 (IPR, NOMA, Sensors, Netw., SPPCom, SOF)*, Optical Society of America, 2016, Paper IW1B.3. [Online]. Available: https://www.osapublishing.org/abstract.cfm?uri=IPRSN-2016-IW1B.3
[21] M. Tien, J. F. Bauters, M. J. R. Heck, D. J. Blumenthal, and J. E. Bowers, "Ultra-low loss Si_3N_4 waveguides with low nonlinearity and high power handling capability," *Opt. Express*, vol. 18, no. 23, pp. 23562–23568, 2010.

Yuan Liu received the M.S. degree in electrical and computer engineering from University of California Santa Barbara (UCSB), Santa Barbara, CA, USA and the M.S. degree in condensed matter physics from the Technical Institute of Physics and Chemistry, Chinese Academy of Sciences, Beijing, China, in 2014 and 2012, respectively. In 2009, he graduated with a B.S. degree from the Harbin Institute of Technology in China. He is currently working toward a Ph.D. degree at UCSB with emphasis on Photonic Integrated Circuits and Microwave Photonics.

Adam Wichman earned the B.S. in electrical engineering with distinction from the United States Naval Academy, Annapolis, MD, USA. He is currently working toward a Ph.D. at Brown University, Providence, RI, USA, where he is a National Defense Science and Engineering Graduate Fellow.

Brandon Isaac received the B.S. degree in physics and chemical engineering from the University of Kentucky, Lexington, KY, USA, in 2013. He spent the first 2 years during his Ph.D. at UCSB working on molecular beam epitaxy for fundamental materials research. He is currently working on high performance opto-electronic devices and photonic integrated circuits for phased arrays applications.

Jean Kalkavage received the M.S. degree in electrical engineering from Boston University, Boston, MA, USA. She is currently with the Johns Hopkins University Applied Physics Laboratory, Laurel, MD, USA. Her experience is concentrated in the technology areas of microwave photonics, digital communications, and photonic integrated circuits. She is an active member of the IEEE Photonics Society.

Eric J. Adles (SM'15) received the B.S. and Ph.D. degrees in physics from North Carolina State University, Raleigh, NC, USA. His graduate research focused on the application of second-harmonic generation for real-time optical diagnostics of semiconductors. From 2009 to 2010, he was a Postdoctoral Researcher at the University of Maryland Baltimore County, Baltimore, MD, USA, where he worked on optoelectronic oscillators and photonic phase noise measurement systems. He is currently a Member of the Principal Professional Staff at the Johns Hopkins University Applied Physics Laboratory, Laurel, MD, USA, where he works on photonic systems for radio frequency and digital communication applications. He is a Member of the IEEE Photonics Society, the Optical Society of America, and the American Physical Society.

Thomas R. Clark, Jr. (M'99–SM'05) received the B.S. degree in physics from Loyola College, Baltimore, MD, USA, the M.S. degree in physics from Lehigh University, Bethlehem, PA, USA, and the Ph.D. degree in physics from the University of Maryland, College Park, MD, USA, in 1991, 1993, and 1998, respectively. He is currently a Supervisor of the Electro-Optical and Infrared Systems and Technologies Group and a member of the Principal Professional Staff at The Johns Hopkins University Applied Physics Laboratory, Laurel, MD, USA. From 1998 to 2000, he was a Research Physicist in the Optical Sciences Division at the Naval Research Laboratory, Washington, DC, USA, where his research interests include the fields of low-noise lasers and microwave photonics. In 2000, he joined the venture-backed Dorsal Networks, Columbia, MD, USA, later acquired by Corvis Corporation, Columbia, MD, USA, where he was a Senior Optical Design Engineer developing hardware and simulation tools for telecommunications applications, including undersea and terrestrial WDM transmission systems, optical amplifiers, optical transceivers, and system control modules. From 2003 to 2010, he was a member of the Senior Professional Staff (2003–2007) and Principal Professional Staff since 2007 at The Johns Hopkins University Applied Physics Laboratory. His research interests include the study of lasers and nonlinear optics, the development and characterization of low-noise and ultrafast photonic systems and devices, and the application of photonics to problems in optical communications and microwave and millimeter-wave systems. He is a member of OSA. He was the 2011 Chair of the OSA/IEEE Optical Fiber Communications subcommittee on Optical Processing and Analog Subsystems, the 2013 co-Technical Program Chair for the IEEE Microwave Photonics Conference and the Chair of the IEEE Photonics Conference subcommittee on Microwave Photonics from 2010 to 2012. He was Technical Program Chair/Member-at- Large/General Program Chair for the 2014/2015/2016 IEEE Photonics Conference.

Jonathan Klamkin received the B.S. degree from Cornell University, Ithaca, NY, USA and the M.S. and Ph.D. degrees from the University of California Santa Barbara, Santa Barbara, CA, USA, in 2002, 2004, and 2008, respectively. From 2008 to 2011, he was a member of the Technical Staff in the Electro-Optical Materials and Devices Group, MIT Lincoln Laboratory, Lexington, MA, USA. From 2011 to 2013, he was an Assistant Professor at the Institute of Communication, Information and Perception Technologies at the Scuola Superiore Sant'Anna, Pisa, Italy. From 2013 to 2015, he was an Assistant Professor of Electrical and Computer Engineering (ECE) and Materials at Boston University, Boston, MA, USA. In 2015, he joined the ECE Department at the University of California Santa Barbara, where he is currently an Associate Professor. He is an Associate Editor for *Photonics Technology Letters* and the Vice Chair for the Microwave Theory and Techniques Society Subcommittee on Microwave Photonics. He was Program Chair for the Integrated Photonics Research, Silicon and Nanophotonics Conference, in 2017, and is serving as General Chair for the same conference, in 2018. He received best paper awards at the 2006 Conference on Optoelectronic and Microelectronic Materials and Devices and the 2007 Microwave Photonics Conference. He also received NASA Early Career Faculty Award. He is a senior member of OSA.